ISBN: 978-3-95450-184-7 doi:10.18429/JACoW-IPAC2018-THPAL052

FINITE ELEMENT ANALYSIS ON BEAM-INDUCED HEAT LOAD IN IN-VACUUM UNDULATORS WITH A SMALL MAGNET GAP

J.C. Chang, Y.H. Liu
National Synchrotron Radiation Research Center, Hsinchu, Taiwan

Abstract

In-vacuum undulators with (IVU) a small gap and short period have been applied in synchrotron accelerators for hard X-rays users for years. However, beam-induced heat load resulted from synchrotron radiation or the image current will not only degrade the performance of undulator but damage the magnet sheet. It is difficult to quantitatively study heat transfer phenomenon of the magnet sheet through physical experiment. In this study, finite element analysis was applied to study the effect of beam-induced heat load on an in-vacuum undulator.

INTRODUCTION

Development of IVU had fulfilled the goal of high-brilliance X-rays in the medium energy storage rings. Moreover, operation at a much smaller magnetic gap can produce higher photon fluxes and brilliance. A short-period undulator with low phase error can make X-ray become a new unprecedented brilliant light source in an ultimate storage ring, which conventional undulators cannot achieve.

In the IVU development progress, KEK had developed IVU in 1991 [1]. ESRF had also installed IVUs since 1999 [2]. Nowadays, IVUs have been developed, installed and in operation around the world. In Taiwan Photon Source (TPS), a 3-GeV synchrotron light source in Taiwan. We have also equipped several short period IVUs in phase I construction and operation.

However, there are some challenge of IVU technologies, which includes phase error issue, counter force system, and heat loss issue [3].

About the heat loss issue, beam-induced heat load is from synchrotron radiation (SR) and image current. Once the magnet sheet is not parallel to the beam direction, maybe resulted from the magnet manufacturing or installation alignment error, it may cause potential risk of avalanche meltdown on a magnet sheet. [4] Heat loss ever made a stainless-steel magnet sheet melt due to resistive wall heating at ESRF. To cope with this wall-heating issue, the stainless steel magnet may be replaced with a cupper sheet [5].

In this study, we took an IVU of TPS as example to simulate the beam-induced heat load and heat transfer phenomenon. In the IVU, the magnet period is 22mm. Thus it was referred to as IU22. A 3D sketch of IU22 and the aluminium I-beam assembly is shown in Fig. 1.

The magnet holders were made of deoxidized copper and fixed on the aluminium I-beam. A copper sheet of 60 micron, coated with nickel of 25 micron covers the magnet array surface to provide suitable impedance on the magnet array. The water cooling pipe firmly attached around the bottom of the aluminium I-beam was designed to remove heat.

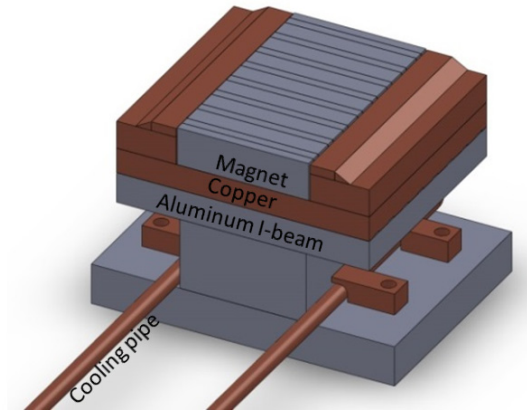

Figure 1: IU22 with holder.

NUMERICAL SIMULATION

CFD began from the early 30s of the 20th century to solve the linearized potential equations with 2D methods. As rapid development of numerical analysis and computer science, CFD has more advantage of well adaptation than traditional theoretical analysis and experimental measurements. Nowadays, CFD has been widely applied in many fields. Detailed 3D numerical simulation was performed using a commercial general purpose CFD code ANASYS Fluent in this study.

Geometry and Grid Generation

Because the geometry of the IU22 and heat transfer condition is symmetric along the beam direction, we built a 3D model of half of IU22 for the numerical simulation. The geometry was built according to the dimensions of the practical IU22, as shown in Fig.2.

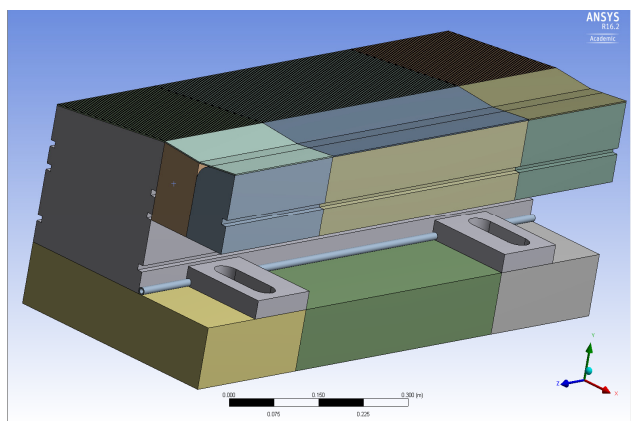

Figure2: Numerical model IU22.

ISBN: 978-3-95450-184-7 doi:10.18429/JACoW-IPAC2018-THPAL052

According to the geometry of the model, we applied hybrid grid to discretize the model. The total number of the grid elements was 944,988. To more accurately giving the thermal boundary condition of heat source and greater control over sizing function, we applied the Advanced Size Function. Figure 3 shows the generated grids of the numerical simulation.

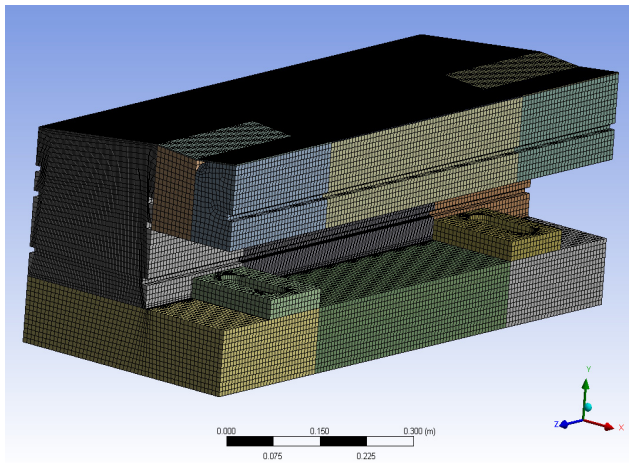

Figure3: Generated grids of the numerical model.

Thermal Boundary Conditions

In this study, heat source of beam-induced heat load includes synchrotron radiation (SR) and image current. For TPS IU22, the main heat loss is from image current. The induced current density [6] may be expressed as

$$j(x)=1/\cosh(x/h) \quad (1)$$

There are two directions of heat transfer onto the magnet sheet. One is the transverse direction where heat transfers from center of the sheet. The other direction of heat transfer is normal through magnet sheet.

In the simulated IU22, the cooling pipe is kept 25 ºC. All other surfaces are assumed adiabatic.

Thermal Resistance

The thermal resistance, R, is related with thickness, d, thermal conductivity, k, and heated surface, A.

$$R = d/kA \quad (2)$$

For a hybrid-typed magnet, the total thermal resistance includes resistance of sheet, magnet and the contact resistance, which is calculated with

$$R_{total} = R_{sheet} + R_{magnet} + R_{contact} \quad (3)$$

where the contact resistance usually dominates the total thermal resistance. In this study, we simulate 5 cases of different contact resistance.

RESULTS AND DISCUSSION

There are two main factors affecting thermal transfer in this study. One is the heat flux from the heat source and the other is the thermal resistance between the magnet and the magnet sheet. We simulate five cases with different thermal resistance between the magnet and the sheet.

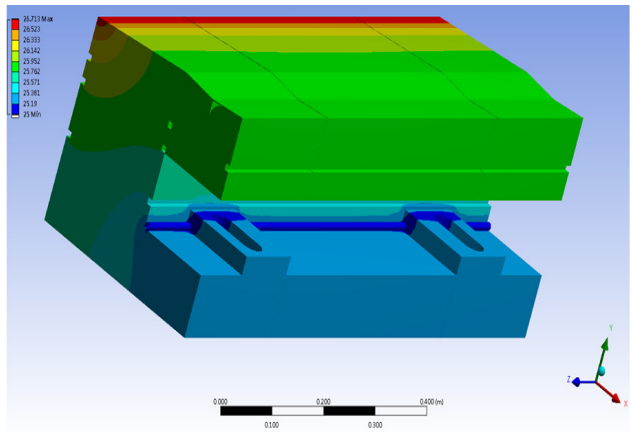

Figure 4: Simulated results without thermal resistance between the magnet and the sheet.

In the first case (case 1), there is no thermal resistance between the magnet and the sheet. The cooling pipe is kept 25 ºC, which is the minimum temperature. The maximum temperature was 26.713 ºC, as shown in Fig. 4. This is a steady state simulation. The final temperature difference between maximum and minimum temperatures is 1.713 ºC .

We also run transient state simulation for case 1. Figure 5 shows maximum temperature history in 1,200 seconds of case 1. The initial temperature is 25 ºC. The maximum temperature rises to 25.93 ºC when time comes to 1,200 seconds.

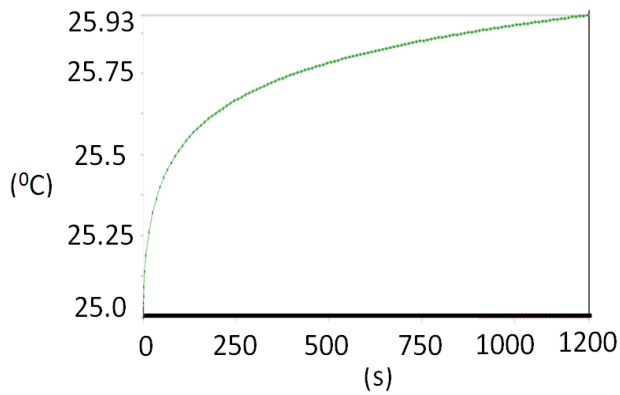

Figure 5: Maximum temperature history of case 1.

In the second case, the thermal resistance between the magnet and the sheet is 0.002 $m^2 \cdot$ ºC/W. In the final steady state condition, the maximum temperature is 28.09 ºC, as shown in Fig. 6. The final temperature difference between maximum and minimum temperatures is 2.09 ºC. Small thermal resistance still affects the temperature distribution more non-uniform than that without thermal resistance. The maximum temperature locates on the middle of magnet, where beam passing through.

ISBN: 978-3-95450-184-7 doi:10.18429/JACoW-IPAC2018-THPAL052

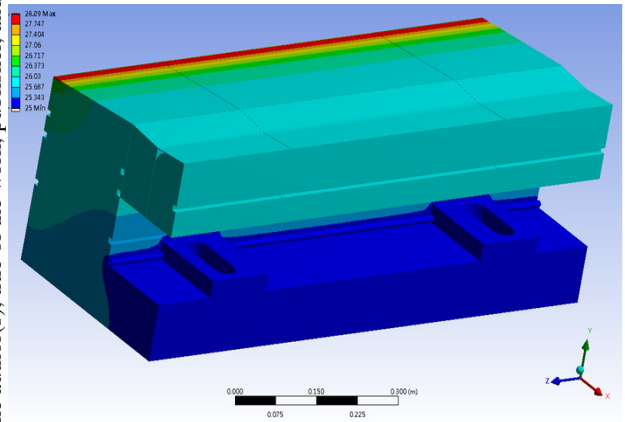

Figure 6: Simulated results with 0.002 $m^2 \cdot °C$ /W thermal resistance between the magnet and the sheet.

Figure 7 shows the simulation case with the thermal resistance between the magnet and the sheet is 0.01 $m^2 \cdot °C$ /W. The maximum temperature was 31.83 °C. The final temperature difference between maximum and minimum temperatures is 6.83 °C. Large temperature gradient also locates on the middle of magnet, as shown in Fig. 7.

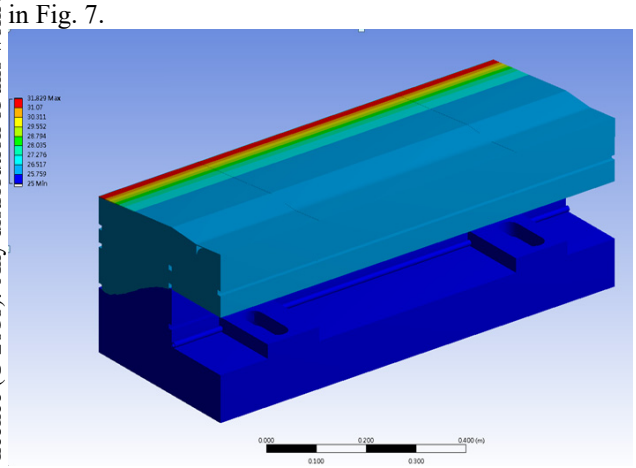

Figure 7: Simulated results with 0.01 $m^2 \cdot °C/W$ thermal resistance between the magnet and the sheet.

Figure 8 shows the simulation case with the thermal resistance between the magnet and the sheet is 0.1 $m^2 \cdot °C/W$. The maximum temperature is 50.927 °C.

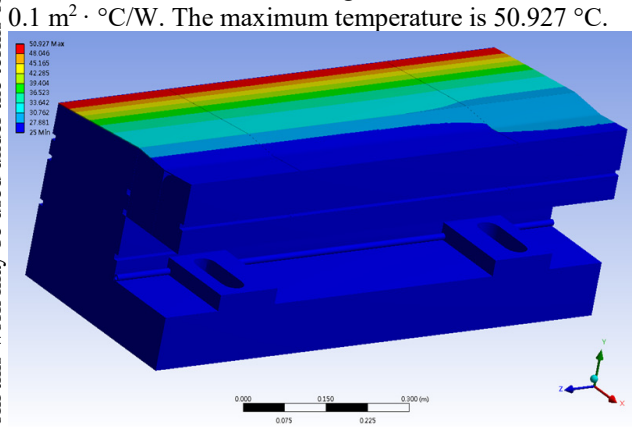

Figure 8: Simulated results with 0.1 $m^2 \cdot °C/W$ thermal resistance between the magnet and the sheet.

Figure 9 shows the simulation case with the thermal resistance between the magnet and the sheet is 1 $m^2 \cdot C/W$. The maximum temperature is 141.02 °C. The final temperature difference between maximum and minimum temperatures is 116.02 °C. The maximum temperature increases with thermal resistance increases. Besides, as thermal resistance increases, heat transfer is mostly on the transvers direction. Therefore, temperature of the magnet (magnet sheet excluded) is close to 25 °C.

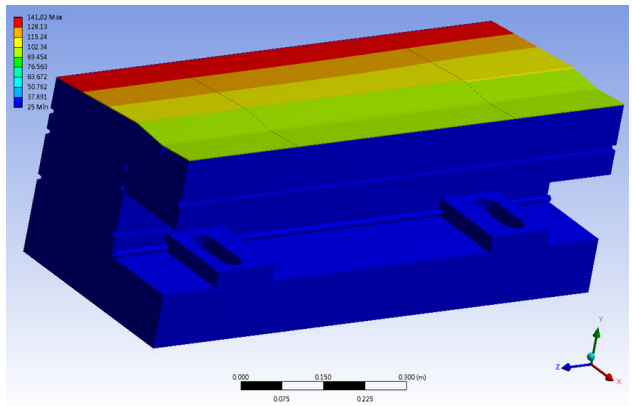

Figure 9: Simulated results with 1 $m^2 \cdot °C/W$ thermal resistance between the magnet and the sheet.

CONCLUSION

In this study, we simulated the heat transfer of IU22 with 5 steady state cases of different contact resistance, including 0, 0.002, 0.01, 0.1 and 1 $m^2 \cdot °C/W$. The maximum temperature ranged from 26.713 to 141.02 °C.

ACKNOWLEDGEMENT

Authors would like to thank J.C. Huang for his valuable discussion and assistance.

REFERENCES

[1] S. Yamamoto *et al.*,"Construction of an In Vacuum Type Undulator for Production of Undulator X-rays in the 5-keV to 25-keV Region", Rev. Sci. Instr., 63, pp. 400-403, 1992.

[2] J. Chavanne *et al.*, "In-Vacuum Undulators at ESRF", in PAC'03, Portland, OR, USA, May 2003, paper TOPA013, pp. 253-255.

[3] Jui-Che Huang *et al.*, "Challenge of In-Vacuum and Cryogenic Undulator Technologies", in *Proc. IPAC'16*, Busan, Korea, May 2016, pp. 1080-1085, doi:10.18429/JACoW-IPAC2016-PAPERID

[4] Jui-Che Huang *et al.*, "Beam-induced Heat Load in In-vacuum Undulators with a Small Magnetic Gap", *Nucl. Instr. Meth.*, 775, pp. 162-167.

[5] T. Hara *et al.*, J. Synchrotron Rad. 5(1998),406.

[6] S. H. Kim, "Optimization of Four-Button BPM Configuration for Small-Gap Beam Chambers," BIW'98, AIP Conf. Proc. 451, 310 (1998).